Pre-normative REsearch for Safe use of Liquid Hydrogen (PRESLHY)

Project Deliverable

D5.2 Computational investigation of combustion phenomena with cryogenic hydrogen

Deliverable Number:	5.2
Work Package:	5
Version:	2.0
Author(s), Institution(s):	D. Cirrone (UU), J. X. Wen (WU), Z. X. Ren (WU); J. Xiao (KIT), M. Kuznetsov (KIT)
Submission Date:	4 June 2021
Due Date:	Month 36
Report Classification:	Public

This project has received funding from the Fuel Cells and Hydrogen 2 Joint Undertaking under the European Union's Horizon 2020 research and innovation programme under grant agreement No 779613.

History		
Nr.	Date	Changes/Author
1.0	6.05.2021	Contribution to Section 2.8 / J. X. Wen, Z. X. Ren (WU)
1.1	16.05.2021	Contribution to Section 2.1-2.7 / D. Cirrone (UU)
1.2	21.05.2021	Contribution to Section 2.1-2.7 / D. Cirrone (UU)
1.3	29.05.2021	Contribution to Section 2.9 / J. Xiao (KIT)
2.0	04.06.2021	Final version / M. Kuznetsov (KIT)

Approvals			
Version	Name	Organisation	Date

Acknowledgements

This project has received funding from the Fuel Cells and Hydrogen 2 Joint Undertaking under the European Union's Horizon 2020 research and innovation programme under grant agreement No 779613.

Key words

Liquid hydrogen, cryogenic hydrogen/air, ignition, jet fire, radiation, combustion pressure, hazard distances.

Publishable summary

The present contribution presents the results on the modelling / computational work and theoretical analysis performed within WP5 “Combustion” of the PRESLHY project. Separate phenomena of cryogenic hydrogen accident scenario, relevant to combustion have been analyzed and numerically simulated: - jet fire behaviour and heat radiation; - pressure peaking phenomena (PPP); - maximum combustion pressure under cryogenic high pressure hydrogen release; - BLEVE. The models, numerical simulations and results of the analysis were validated against experiments performed within PRESLHY project as well as known experiments from the literature. The extension of the numerical simulations and analytical results to real accident scenarios with respect to safety distances evaluation was provided then as engineering tools guideline.

Abbreviations

GH2	Gaseous Hydrogen
LH2	Liquefied Hydrogen
CFD	Computational Fluid Dynamics
BLEVE	Boiling Liquid Expanding Vapour Explosion
IR	Infrared
LFL	Lower Flammable Limit
RCS	Recommendations Codes and Standards
RH	Relative Humidity

Table of Contents

List of figures

List of tables

1 Introduction and scope

Work package 5 (WP5) of PRESLHY project is dedicated to cryogenic hydrogen combustion experiments, analysis and computations. The theory of cryogenic hydrogen combustion is based on general combustion theory with the difference that the state of combustible matter can be condensed, two-phase or gaseous but in all the cases at least non-ideal and the real gas equation of state (RG EoS) should be accounted. Independent of lower chemical reactivity at cryogenic temperatures the danger of cryogenic hydrogen combustion should be stronger than hydrogen combustion at ambient temperature because of 3-5 times higher density of combustible matters. How the density factor balances against the lower chemical reactivity at cryogenic temperatures is of the great practical importance.

Not all the accident combustion phenomena can be experimentally reproduced due to the complexity of the processes or unavoidable dangerous consequences lead to the failure of surrounding structures or human victims, especially in the cases if approaching the real scale. Then, it needs numerical simulation of such processes to finally complete the analytical research to create reliable models and parametric correlations for safety assessment. Within the numerical simulation part, several combustion phenomena have been investigated in detail:

- Jet fire behaviour and its thermal radiation. A hazard diagram of heat radiation effect on human skin and safety distances evaluation was derived on the basis of numerical simulations and experimental validation of the model.
- Flame length correlation for a stationary jet fire to be used as a scaling factor for safety distance evaluation in the processes of heat radiation for hydrogen jet fires.
- The ignition of high pressure cryogenic hydrogen with respect to maximum combustion pressure were numerically studied and validated against PRESLHY experiments and also involving the known reference data.
- Flame behaviour after jet ignition was numerically investigated regarding the flash back phenomena, governing the further flame extension and steady jet fire formation or extinction of the flame.
- Pressure peaking phenomena (PPP) analysis and modelling in order to evaluate the maximum possible pressure occurred due to cryogenic hydrogen release and combustion in an enclosure with vent orifice.
- BLEVE phenomenon analysis and semi-empirical correlation for maximum dimension of the fireball produced by the BLEVE process.

The report gathers the results on numerical simulations to be used for engineering correlations and tools development and also for RCS recommendations.

The scope of the deliverable is the following:

- To provide the results of numerical simulations and experimental validation on the cryogenic hydrogen combustion, to propose engineering correlations and to calculate the hazard distances of relevant accident scenarios. Such engineering correlations will be fed into recommendations for Regulations, Codes and Standards.

2 Numerical simulations and analysis

2.1 Thermal radiation from cryogenic hydrogen jet fires (UU)

Jet flames originated by cryo-compressed ignited hydrogen releases can cause life-threatening conditions in their surroundings. Understanding of consequences of potential accidents with cryogenic hydrogen jet fires is fundamental to protect life and prevent property loss. Panda and Hecht (2017) observed that, for a fixed mass flow rate, the decrease of release temperature causes a longer flame length and higher radiative heat flux from a jet flame. Ulster University performed a computational study to develop and validate a CFD model to simulate flame length and radiative heat flux for cryogenic hydrogen jet fires. Simulation results are used to assess thermal hazard distances for vertical and horizontal cryogenic jet fires.

The CFD approach employs an implicit pressure-based solver and incompressible ideal gas flow. A Reynolds-Averaged Navier–Stokes (RANS) approach is employed with the realizable κ-ε sub-model for solving turbulent kinetic energy and turbulent dissipation rate (Shih et al., 1995). The Eddy Dissipation Concept is used for combustion modelling (Magnussen, 1981). It includes detailed chemical mechanisms of 9 species and 18 reactions by a subset of Peters and Rogg's mechanisms (Peters and Rogg, 1993). The Discrete Ordinates model is implemented to take into account radiation losses (Murthy and Mathur, 1998). Detailed description of governing equations is available in (Cirrone et al., 2019a).

Experiments on hydrogen jet fires in (Panda and Hecht, 2017) and (Breitung et al., 2009) were used to validate the CFD approach against measurements of flame length and radiative heat flux at several locations from the jet fire. The notional nozzle approach by (Molkov et al., 2009) was used to model the release sources. Figure 1 shows the comparison of simulation results against 5 tests performed at SNL. Experimental radiative heat flux was predicted with ±15% accuracy; only exceptions are given at the 5th sensor in 2 tests. Experimental flame length was predicted with an accuracy within 14%. Full description of computational studies and results is reported in (Cirrone et al., 2019a).

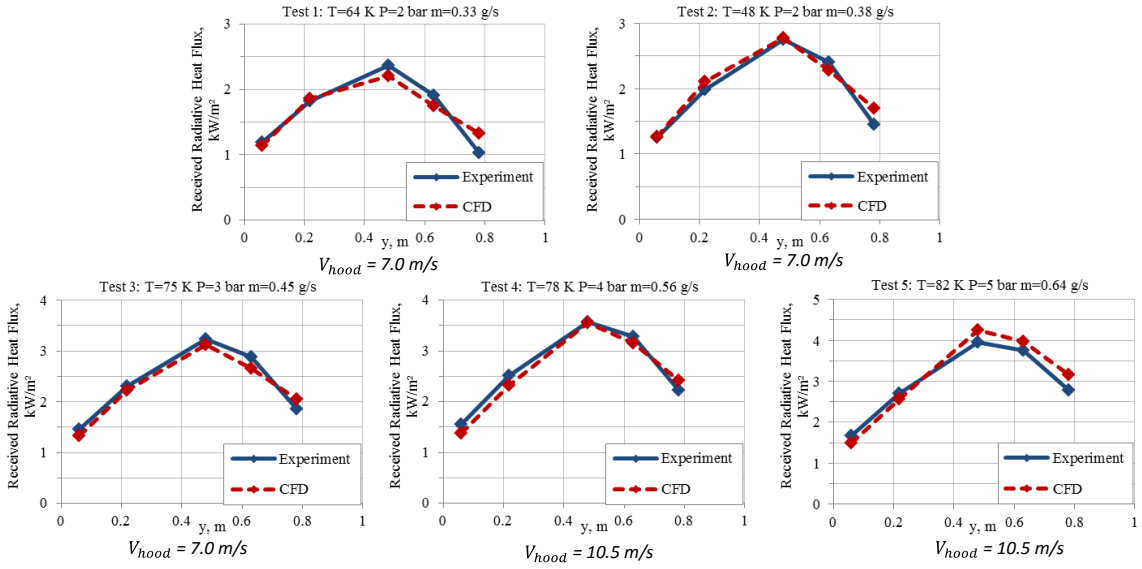

Figure 1. Radiative heat flux evaluation for SNL validation experiments (Cirrone et al., 2019a).

The thermal dose in the near field of the simulated jet fires was estimated in (Cirrone et al., 2019b) for several exposure times. The harm criteria for people were defined according to the thermal dose thresholds for infrared radiation. It was found that for Tests 1-3 the maximum exposure time to not be "harmed" at 0.5 m from the flame axis should be lower than 30 s, as shown in Figure 2 reporting the harm degree as function of time and distance from the flame axis. In test 3 an exposure prolonged to 60 s resulted in second degree burns at 0.5 m from the jet flame

axis. At the same distance, 4 minutes is the maximum exposure time before third degree burns occurrence.

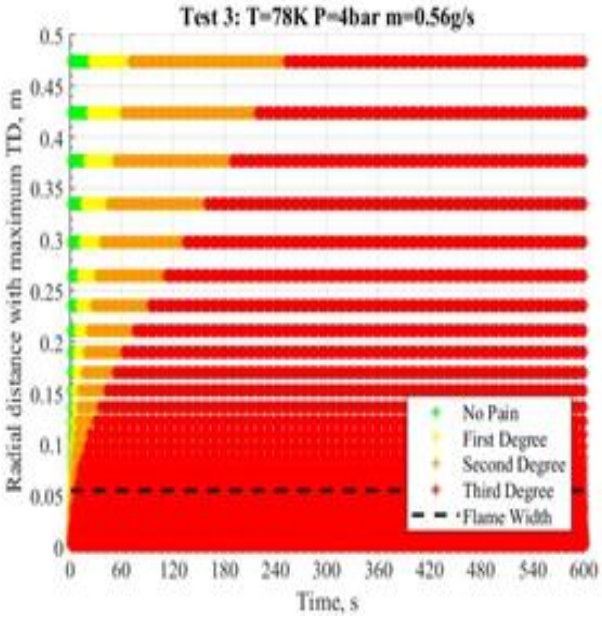

Figure 2. Thermal dose harm levels: time versus radial distance with maximum TD.

The CFD model validation was extended to horizontal cryogenic jet fires experiments performed by (Breitung et al., 2009). In this case the release source was modelled by the notional nozzle approach with inclusion of heat transfer effect by means of numerical simulations (see Cirrone et al., 2021). Figure 3 shows the comparison of the simulated and experimental radiative heat flux measured at different locations from the jet fire. Simulation results of Test 3 with a relative humidity (Rh) equal to 77% well agree with experiments with accuracy within 10%. Few exceptions are observed at distances from the jet axis z=50cm and z=125cm. For Test 4, prediction accuracy of simulations is within 20%, with exceptions of sensors at z=125cm. Simulations for Rh=77% underestimate the measured radiative heat flux for both tests at z=125cm. Predictions from simulations for Rh=50%, which is the value generally maintained in controlled environments, overlap with experiments at z=125cm. These outcomes suggest a possible non uniform relative humidity distribution in the chamber.

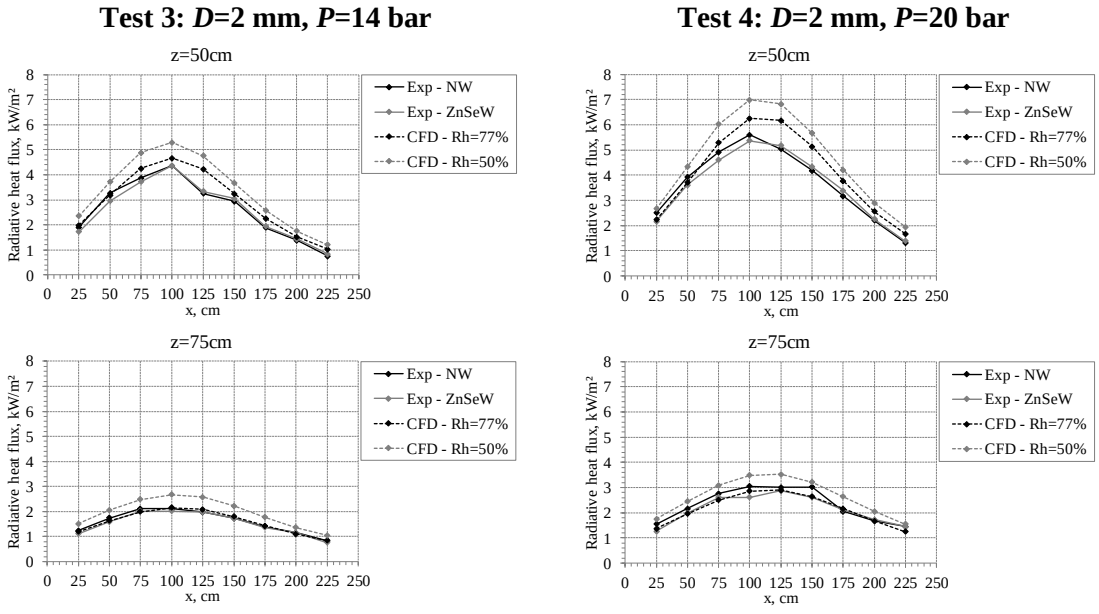

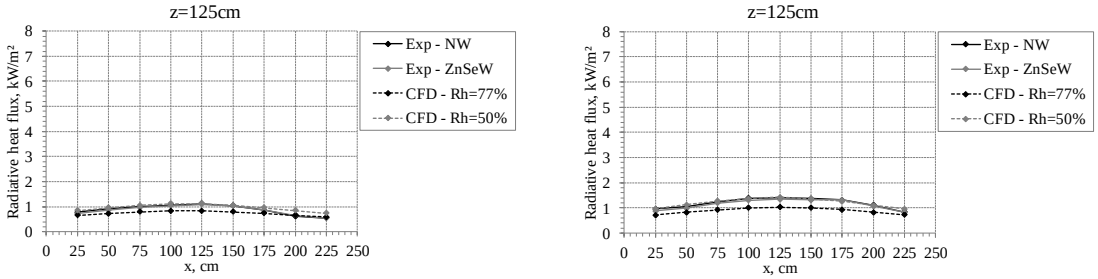

Figure 3. Radiative heat flux evaluation for KIT validation experiments: Tests 3-4 (Cirrone et al., 2021).

Figure 4 presents the simulation results for Tests 5 and 6. Prediction accuracy for Test 5 (Rh=77%) is within 10% for sensors at z=50 cm. Experimental measurements at z=125cm are underpredicted by simulations. The use of Rh=50% considerably improve predictions at z=75cm, and overlap with experiments at z=125cm, as observed for Tests 3 and 4. For Test 6 (Rh=77%) simulation underestimates experimental measurements beyond x=100 cm. This is consistent with the underprediction of flame length, yet within acceptable 15% variation.

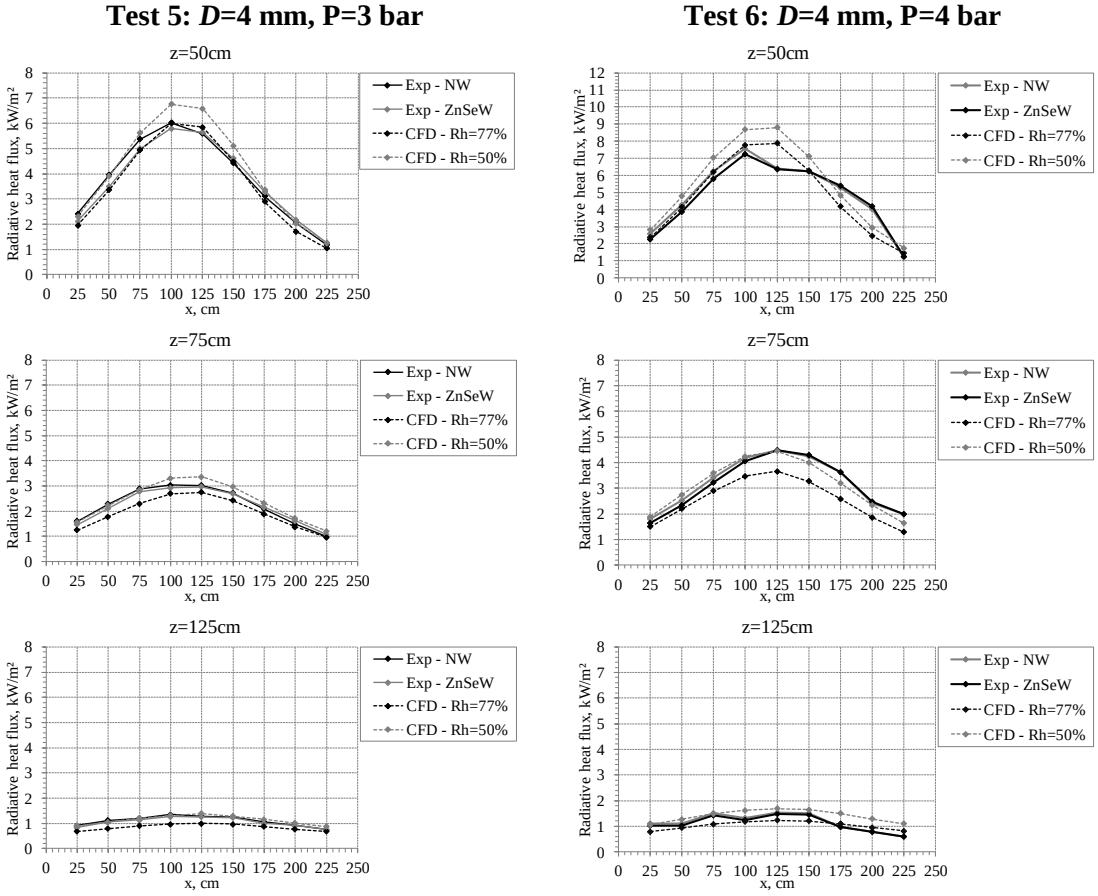

Figure 4. Radiative heat flux evaluation for KIT validation experiments: Tests 5-6 (Cirrone et al., 2021).

A jet fire leads to the production of hot currents harmful to people. (Molkov, 2012) correlated the temperature distribution along a vertical hydrogen fire trajectory from experiments available in literature to the distance normalised by the flame length in order to derive hazard distances for people. However, in simulations of horizontal jet fires the flame and combustion products distributions were seen to be affected by buoyancy. As a result, the buoyancy of combustion

products considerably reduces the "no harm" distance from x=3.5L_f for vertical jet fires to x=2.2L_f for horizontal jet fires (see Table 1). Hazard distance by "fatality" limit decreases from x=2.0L_f to x=1.75L_f. However, it should be highlighted that conclusions and change of multiplier in hazard distance between vertical and horizontal jet are valid for these particular tests.

Table 1. Hazard distances for vertical and horizontal jet fires by temperature criteria (*along the flame tilting axis).

Harm level (LaChance et al., 2011)	Hazard distances	
	Vertical jet fires	Horizontal jet fires*
"No-harm": 70°C for any exposure duration	x=3.5L_f	x=2.2L_f
"Pain": 115°C for 5 minutes exposure	x=3L_f	x=2.1L_f
"Fatality": 309°C, third-degree burns for 20 s exposure	x=2L_f	x=1.75L_f

The analysis was extended to the assessment of hazard distances by thermal radiation criteria (Lachance et al., 2011). It was found that thermal radiation leads to longer "no-harm" distances in the direction of the jet (x=3.0-3.2L_f) compared to hazard distance defined by temperature for horizontal jet fires (=2.2L_f). Harmful distances on the side of the investigated experimental jets were calculated to be longer than the domain size, i.e. 2.7 m in the radial direction to the jet. "First-degree burns" hazard distance (4.0 kW/m^2) along the jet fire direction was found to be x=2.1L_f. "First-degree burns" hazard distance (4.0 kW/m^2) on the side of the horizontal jet fire is about 3.5 times shorter than hazard distance in axial direction. Finally, the study assessed the thermal dose in the jet fire surroundings. The thermal dose calculates the harm level as a function of exposure duration and incident thermal radiation, and is a valuable tool to assess the feasibility of short-term activities and emergency operations. Simulation results suggest that firefighters can stand without harm as close as 0.71 m to the jet fire axis for a time < 168 s. All results and throughout description of the performed study are available in (Cirrone et al., 2021).

2.1.1 Concluding remarks

The CFD model for simulation of thermal hazards from cryogenic hydrogen jet fires is validated against experiments with release temperatures in the range 48-82 K and pressures up to 20 bar. It was observed that the buoyancy of combustion products reduces the "no harm" distance by temperature from x=3.5L_f for vertical jet fires to x=2.2L_f for the investigated horizontal jet fires. For horizontal jet fires, thermal radiation leads to longer "no-harm" distances in the direction of the jet (x=3.2L_f) compared to hazard distance defined by temperature. Harmful distances on the side of the investigated horizontal jets were calculated to be longer than the domain size, i.e. 2.7 m in the radial direction to the jet. The thermal dose is a useful parameter to define hazard distances for emergency personnel. A throughout assessment of thermal hazards and associated distances from a hydrogen jet fire should combine the analysis of temperature, thermal radiation and thermal dose, as these are found to be complementary to each other.

2.2 Pressure Peaking Phenomenon for ignited cryogenic hydrogen releases (UU)

Releases of hydrogen in a confined space with limited ventilation can produce a transient pressure dynamics with a distinctive peak exceeding the steady state pressure. This is defined as pressure

peaking phenomenon (PPP), and is particularly pronounced for hydrogen as characterised by the lowest density. The magnitude of the peak pressure depends mainly on hydrogen release rate, ventilation rate and enclosure volume. The phenomenon was firstly described theoretically in (Brennan et al., 2010) for unignited hydrogen releases. It was found that the produced peak pressure in an enclosure could be significantly higher than thresholds for preventing destruction of civil structures (10-20 kPa). PPP may be relevant in case of a fire involving a hydrogen vehicle parked in a residential garage, following the venting of high pressure gas through the non-reclosing thermally-activated pressure relief device (TPRD) on the storage tank. In such a case, hydrogen is likely to ignite, leading to a more pronounced PPP compared to unignited releases, as observed in (Makarov et al., 2018). Numerous experimental, analytical and numerical works have been performed on PPP originated by releases of warm hydrogen, see (Brennan and Molkov, 2013), (Brennan and Molkov, 2018), (Makarov et al., 2018), (Lach et al., 2020), (Lach et al., 2021), (Hussein et al., 2018), (Brennan et al., 2019). Ulster University performed a numerical assessment of pressure peaking phenomenon (PPP) for cryogenic hydrogen ignited releases in a garage-like scenario. The effect of storage hydrogen temperature was investigated by changing it from ambient to 200 and 100 K, by maintaining either the same discharge coefficient or mass flow rate as for the ambient temperature release.

A Computational Fluid Dynamics (CFD) model previously validated against small scale experiments (Hussein et al., 2018) is employed here. The CFD approach employs an implicit pressure-based solver and compressible ideal gas flow. A Reynolds-Averaged Navier–Stokes (RANS) approach is employed with the realizable κ-ε sub-model for solving turbulent kinetic energy and turbulent dissipation rate (Shih et al., 1995). The Eddy Dissipation Concept is used for combustion modelling (Magnussen, 1981). It includes detailed chemical mechanisms of 9 species and 18 reactions by a subset of Peters and Rogg's mechanisms (Peters and Rogg, 1993). The Discrete Ordinates model is implemented to take into account radiation losses (Murthy and Mathur, 1998). Detailed description of governing equations is available in (Hussein et al., 2018).

2.2.1 CFD model validation against ambient temperature experiments

The CFD model was firstly validated against ambient temperature tests performed by the Universitetet I Sorost-Norge (USN) in a chamber with volume 15 m^3. Tests were conducted within the frame of HyTunnel-CS project and details are given in (Lach et al., 2020; 2021). Thirty-one tests were conducted on ignited hydrogen releases with mass flow rate up to 11.72 g/s. The recorded maximum overpressure was approximately 48 kPa. The chamber had three openings for venting combustion products, which were fully closed or opened according to the desired venting area for each test. Three tests were selected for the validation of the CFD model with highest mass flow rate (up to 11.37 g/s) and recorded overpressure for each of the open vents scenarios, i.e. 1, 2 or 3 vents open. Storage pressure reached 12.46 MPa. At such value, an under-expanded jet is expected, thus a volumetric source approach is used to model the hydrogen jet in simulations (Molkov et al., 2009). A discharge coefficient, C_d, is introduced into calculations to take into account the pressure and local losses in the release pipe and orifice system, and it is found to be 0.12-0.13.

The computational domain has dimensions 6.0x3.5x5.0m. The release source is modelled as one cubic cell with length 3.8 cm. The total number of control volumes in the domain is 235881. Simulations were performed on Ansys Fluent v19.2. Hydrogen conditions at the release are constant in time. Therefore, in the present case, setting a constant time step during hydrogen release is equivalent to set a constant CFL. Convergence by CFL was found for a value equal to 0.75, which corresponds to a time step (ts) of 0.25ms. A further decrease of CFL to 0.37 (ts=0.125 ms) results in a variation of peak overpressure by 0.7%, which is considered to be negligible.

Simulation of test with P=11.78 MPa, $\dot{m}$=11.37 g/s, N. vents=3, resulted in a pressure peak equal to 20.9 kPa, which well agrees with experimentally measured 21.1 kPa. The experimental pressure dynamics is well reproduced. Simulated negative overpressure decreases up to about -3 kPa, whereas experiment measured about -4 kPa.

The CFD model was applied to two further tests. Simulation of test with P=12.46 MPa, $\dot{m}$=11.47 g/s, N. vents=2 resulted in a pressure peak of 35.10 kPa, which conservatively predicts the experimentally measured 33.22 kPa within 7% accuracy. On the other hand, simulated overpressure in the enclosure for test with P=8.93 MPa, $\dot{m}$=8.62 g/s, N. vents=1, reaches a maximum value of 42.21 kPa, which underpredicts the experimental pressure peak (48.1 kPa) by 14%. The magnitude of the pressure negative phase was well predicted for both tests. Full description and discussion of results is available in (Markert et al., 2020).

2.2.2 Pressure peaking phenomenon for cryogenic hydrogen releases

Hydrogen may be stored in cryo-compressed conditions, i.e. storage temperature below 120 K as generally considered for cryogenics (Radebaugh, 2002) and pressure up to 35 MPa (Ahluwalia et al., 2016). For the same storage pressure and release nozzle, a decrease of temperature in the storage would lead to higher hydrogen mass flow rate at the release, and as a consequence, greater peak pressure in the enclosure. The present section assesses the effect of storage temperature decrease on the resulting PPP dynamics for the same enclosure and CFD modelling parameters used for validation against ambient temperature releases. The selected scenario has storage pressure 11.78 MPa and nozzle diameter 4 mm. All the three vents of the enclosure are fully open. The storage temperature, T_S, is varied from 277 K to an intermediate temperature of 200 K and to cryogenic temperature of 100 K. Four cases are simulated, and details are given in Table 2. Parameters at the notional nozzle are calculated through the under-expanded jet theory implementing NIST EOS as presented in (Cirrone et al., 2019c). Cases 2 and 3 maintain the same discharge coefficient as per ambient temperature test. The decrease of temperature causes an increase of released hydrogen from 11.37 g/s for T_S=277 K, to 14.11 g/s for T_S=200 K and 23.16 g/s for T_S=100K. Cases 4 and 5 isolate the effect of only storage temperature on the PPP dynamics by maintaining the same mass flow rate as per Case 1. As a consequence, discharge coefficient is changed to match Case 1 mass flow rate. A CFL=0.75 is used for all simulations.

Table 2. Simulations to assess effect of storage temperature on PPP: storage, release and notional nozzle conditions.

Case	Storage pressure, MPa	Storage temperature, K	C_d	Mass flow rate, g/s	D_{not}, mm	T_{not}, K	U_{not}, m/s
1	11.78	277	0.13	11.37	11.0	230.8	1154.5
2	11.78	200	0.13	14.11	10.8	145.0	915.1
3	11.78	100	0.13	23.16	11.1	67.3	623.3
4	11.78	200	0.10	11.37	9.7	145.02	915.1
5	11.78	100	0.06	11.37	7.8	67.3	623.3

Figure 5. Effect of cryogenic temperature on overpressure dynamics in the enclosure.

 presents the resulting overpressure dynamics for the simulated cases (see Table 2). As expected, simulated cases 2 and 3 present a higher peak pressure, due to the higher hydrogen mass flow rate. The peak pressure recorded for case 2 is 26.95 kPa. The peak pressure increases up to 42.82 kPa for a hydrogen mass flow rate equal to 23.16 g/s. To a higher peak pressure corresponds a more pronounced underpressure, which reaches -5.36 kPa.

Cases 4 and 5 investigates the effect of hydrogen storage temperature on pressure peaking phenomenon while maintaining the mass of released hydrogen the same as in case 1 by reducing the discharge coefficient. Reduction of temperature leads to a slight decrease of peak pressure in the enclosure from 20.95 kPa for T_S=277 K to 20.51 kPa for T_S=200 K and to 19.96 kPa to T_S=100 K. This result is expected as a decrease of the hydrogen temperature mixing with air would lead to a decrease of temperature in combustion. As an example, the adiabatic combustion temperature for a stoichiometric hydrogen-air mixture would decrease from 2388.3 K to 2283.48 K when the mixture initial temperature is decreased from 298 K to 100 K (Reaction Design, 2016). As a consequence, after stopping the hydrogen release, combustion products cool down

faster for lower hydrogen release temperature. This causes a more pronounced negative pressure as shown in Figure 5.

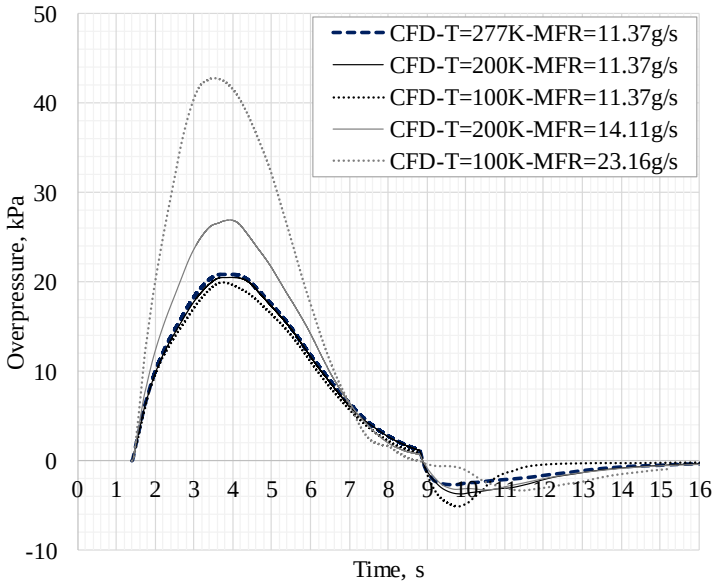

Figure 5. Effect of cryogenic temperature on overpressure dynamics in the enclosure.

2.2.3 Concluding remarks

The pressure peaking phenomenon following ignited hydrogen releases in an enclosure with limited ventilation was investigated by means of numerical simulations. The CFD approach was firstly validated against unprecedented large scale experimental tests in a chamber with volume 15 m^3 with hydrogen releases with storage pressure up to 12 MPa and mass flow rate up to 11.5 g/s. Peak overpressure as large as 48 kPa was recorded in experimental tests. Experimental peak pressure was predicted with accuracy ±14%, which is considered to be within acceptable engineering accuracy. The tool can be employed in hydrogen safety engineering to determine PPP in enclosure and assess release parameters to prevent damage to structures.

The developed and validated approach was applied to assess the effect of cryogenic storage temperature on PPP from ignited hydrogen releases. As expected, the decrease of storage temperature for a same discharge coefficient caused an increase in hydrogen mass flow rate, and, thus, higher peak overpressure. It was found that for a storage pressure equal to 11.78 MPa, the peak overpressure increased from 20.95 kPa to 42.82 kPa for a temperature reduction from 277 K to 100 K. This effect should be considered in design of TPRD size for cryo-compressed hydrogen storages.

2.3 BLEVE (UU)

Ulster University developed an original modelling approach and performed CFD simulations of what is called the boiling liquid expanding vapour explosion (BLEVE) of LH2 storage vessels. A CFD model similar to that validated against the USA and Japanese tests on the rupture of a high-pressure gaseous hydrogen storage tank in a fire (Molkov et al., 2021) was applied after the adaptation to reproduce the LH2 tank explosions performed experimentally by BMW (Pehr, 1996). The CFD model accounts for the contribution of hydrogen reaction with air to the blast wave strength. Simulations were compared to experiments performed by BMW, which included tests with storage pressure in the range 2-11 bar and mass of hydrogen in the tank within the range 1.8-5.4 kg. Figure 6 shows the preliminary results of CFD simulations against experimental pressures. The employed CFD model reproduces with excellent agreement experiments at an

initial pressure of 11 bar and underpredicts one of two experiments at initial pressure 2 bar. Further research will be performed to understand this underprediction and advance the CFD approach and gain insights into the modelling of LH2 BLEVE.

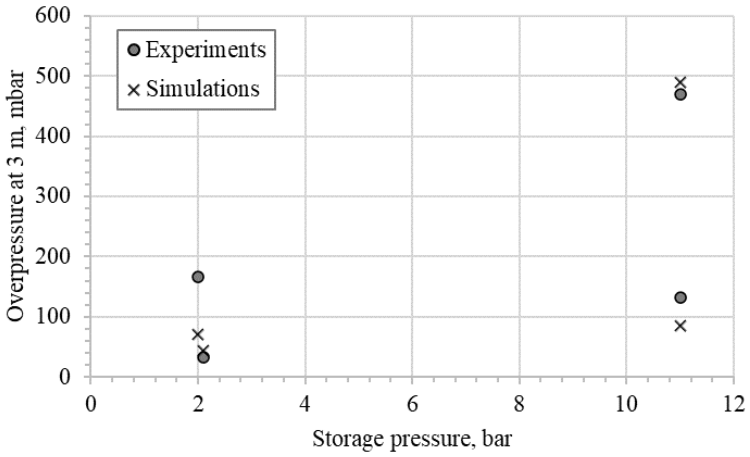

Figure 6. Simulated and experimental overpressure by BLEVE of a LH2 storage tank.

2.4 Flame length correlation and hazard distances for hydrogen jet fires (UU)

The dimensionless flame length correlation is described in detail in (Saffers and Molkov, 2013). The correlation is valid for laminar and turbulent flames, buoyancy - and momentum-controlled fires, expanded (subsonic and sonic) and under-expanded (sonic and supersonic) jet fires. The dimensionless correlation for hydrogen jet flames was validated against jet fires with pressure in the range 10-900 bar and temperature in the range 187-300 K (Saffers and Molkov, 2013). Within the frame of PRESLHY project, Ulster University expanded the validation range of the correlation to jet fires with release temperature down to 46 K for pressure up to 6 bar abs against experiments by (Panda and Hecht, 2017), see (Cirrone et al., 2019c). Figure 7 shows the dimensionless hydrogen flame length correlation against the experimental data employed for a validation of the tool. The flame length normalized to the release diameter L_f/d depends only on the release conditions at the nozzle exit, i.e. density ρ_N and velocity u_N, the corresponding speed of sound, C_N, and the density of the surrounding air, ρ_s, grouped in the following dimensionless quantity:

$$X = \frac{\rho_N}{\rho_s} \cdot \left(\frac{u_N}{C_N}\right)^3$$

Parameters at the nozzle exit can be calculated through the under-expanded jet theory developed at Ulster and validated as well against the cryogenic releases included in the validation range of the flame correlation (Cirrone et al., 2019c).

(Molkov, 2012) compared the distribution of axial temperature along the axis, measured in experiments on vertical hydrogen jet fires by (Imamura et al., 2008), (Barlow and Carter, 1996) and (LaChance, 2010), as function of the distance normalised to the flame length against three harm criteria defined by (LaChance, 2010). It was found that hazard distances by temperature harm criteria can be defined as follows:

- No harm (70°C) hazard distance, $X_{70} = 3.5L_f$;

- Pain limit (5 mins, 115°C) hazard distance, $X_{115} = 3L_f$;
- Third degree burns (20 sec, 309°C) hazard distance, $X_{309} = 2L_f$.

The tool is available on e-laboratory platform developed within Net-Tools (https://elab-prod.iket.kit.edu/).

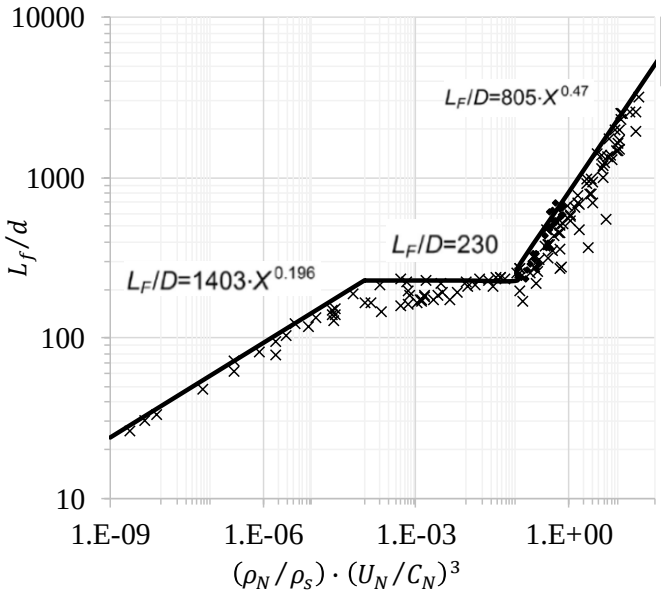

Figure 7. The dimensionless correlation for hydrogen jet flames: "+" data from Saffers and Molkov (2013); "♦" data from Cirrone et al. (2019c).

2.5 Assessment of thermal load from hydrogen jet fires (UU)

Hydrogen jet flames may pose hazardous conditions in their surroundings due to the emitted thermal radiation. Ulster University proposed an engineering tool to assess the radiative heat flux in the surrounding of hydrogen jet fires from vertical and horizontal releases of hydrogen at ambient and cryogenic temperature. The model is based on the weighted multi source flame radiation model developed by (Hankinson and Lowesmith, 2012), which was further expanded by (Ekoto et al., 2014) for application to large scale flames. Within the framework of PRESLHY project, Ulster University adapted the model to include evaluation of hydrogen release parameters at the nozzle according to theory by (Molkov et al., 2009), estimation of flame length and width through the dimensionless correlation by (Saffers and Molkov, 2013), and to expand its validation and applicability range to cryogenic hydrogen jet fires. The model description and validation is presented in detail in (PRESLHY D6.5, 2021). Overall, three experimental series for a total of 12 tests were used to validate the engineering model to assess the radiative heat flux at several distances from the hydrogen jet fire:

- Sandia National Laboratories tests (Panda and Hecht, 2017): 5 tests with storage temperature in the range 48-92 K, storage pressure up to 5 bar and nozzle diameter equal to 1.25 mm;
- KIT tests (Breitung et al., 2009): 6 tests with storage temperature equal to either 80 K or 290 K, storage pressure up to 20 bar and nozzle diameters equal to 2 and 4 mm;
- INERIS tests (Proust et al., 2011): 1 test on hydrogen transient release during blowdown of a storage tank with initial temperature 315 K, initial pressure 900 bar and release nozzle diameter 2 mm.

The discussion of the model results and validation against experiments is presented in detail in (PRESLHY D6.5, 2021). Overall, the model was found to well predict experimental

measurements for the wide range of storage and release conditions. Figure 8 shows an example of the model predictions of radiative heat flux versus experimental measurements by (Breitung et al., 2009) for a cryogenic hydrogen jet fire with release temperature 80 K.

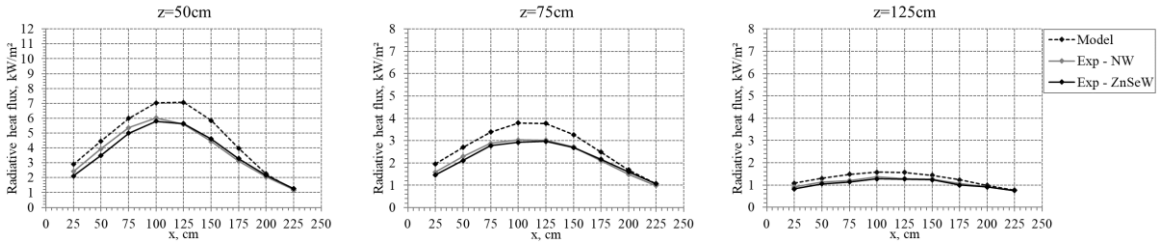

Figure 8. Validation of the model against KIT test with T=80 K, P=3 bar, d=4 mm: calculated versus experimental radiative heat flux.

In conclusion the model allows to predict accurately the radiative heat flux from hydrogen jet fires by knowing only the storage conditions and nozzle diameter. The model can be used to calculate hazard distances according to harm criteria available in literature, and the received thermal dose for a certain exposure duration.

2.6 Maximum pressure load from delayed ignition of turbulent jets (UU)

The delayed ignition of a highly turbulent under-expanded hydrogen jet may cause a strong deflagration. The generated overpressure can seriously harm people and damage civil structures. Ulster University developed a semi-empirical correlation to predict the maximum overpressure generated by delayed ignition of a hydrogen jet at an arbitrary location for known storage pressure, temperature and release diameter. The correlation is applicable only to free jets in open atmosphere.

The similitude analysis has been applied to build a correlation. The dimensionless overpressure generated by delayed ignition of hydrogen jets at an arbitrary location, $\Delta P_{exp}/P_0$, is correlated to the dimensionless parameter composed of the product of the dimensionless storage pressure, $\sqrt{P_s/P_0}$, and the square of ratio of release diameter to the distance between the centre of the fast burning mixture in the jet (25-35% by volume) and the target location, $(d/R_w)^2$. For cryogenic jets, the correlation includes dependency on a corrective factor calculated from the release and ambient temperatures, and the associated expansion coefficients' ratio. The assumptions and detailed description of the model are given in (PRESLHY D6.5, 2021).

Data from approximately 80 experimental tests, with hydrogen storage pressure 0.5-65 MPa and release diameter 0.5-52.5 mm, were used to build the correlation: (Royle and Willoughby, 2010); (Grune et al., 2013); (Grune, 2019); (Takeno et al., 2007); (Takeno, 2019); (Daubech et al., 2015); (Miller et al., 2015). Experimental data of tests conducted within PRESLHY by Pro-Science and KIT were used to expand the applicability range of the correlation to cryogenic temperature of a release (Friedrich et al., 2021).

It is well known that the overpressure generated by delayed ignition of hydrogen jets strongly depends on ignition delay and location, as these factors determine whether ignition verifies in a hydrogen rich or lean portion of the jet, or in a more or less unsteady and turbulent zone. Therefore, it is relevant to highlight that the main practical objective of the study has been the derivation of an experimentally based conservative correlation for determining the maximum overpressure that could be produced by delayed ignition of any hydrogen jet for arbitrary ignition conditions.

2.7 References (UU)

Ahluwalia, R.K., Peng, J.-K., Hua, T.Q., 2016. Cryo-compressed hydrogen storage. In: Gupta,

R.B., Basile, A., Veziroğlu, T.N. (Eds.), Compendium of Hydrogen Energy. T.Q., pp. 119–145.

Barlow, R.S., Carter, C.D., 1996. Relationship among nitric oxide, temperature and mixture fraction in hydrogen jet flames. Combust. Flame 104, 288–299.

Breitung, W., Stern, G., Veser, A., Friedrich, A., Kutznetsov, M., Fast, G., Oechsler, B., Kotchourko, N., Travis, J.R., Xiao, J., Schwall, M., Rottenecker, M., 2009. Final Report:Experimental and theoretical investigations of sonic hydrogen discharge and jet flames from small breaks, KIT / Research Center Karlsruhe.

Brennan, S., Hussein, H.G., Makarov, D., Shentsov, V., Molkov, V., 2019. Pressure effects of an ignited release from onboard storage in a garage with a single vent. Int. J. Hydrogen Energy 8927–8934.

Brennan, S., Makarov, D., Molkov, V., 2010. Dynamics of Flammable Hydrogen-Air Mixture Formation in an Enclosure with a Single Vent. In: Sixth International Seminar on Fire and Explosion Hazards.

Brennan, S., Molkov, V., 2013. Safety assessment of unignited hydrogen discharge from onboard storage in garages with low levels of natural ventilation. Int. J. Hydrogen Energy 38, 8159–8166.

Brennan, S., Molkov, V., 2018. Pressure peaking phenomenon for indoor hydrogen releases. Int. J. Hydrogen Energy 43, 18530–18541.

Cirrone, D., Makarov, D., Kuznetsov, M., Friedrich, A., Molkov, V., 2021. Effect of heat transfer through the release pipe on simulations of cryogenic hydrogen jet fires and hazard distances. In: International Conference on Hydrogen Safety.

Cirrone, D., Makarov, D., Molkov, V., 2019a. Thermal radiation from cryogenic hydrogen jet fires. Int. J. Hydrogen Energy 44, 8874–8885.

Cirrone, D., Makarov, D., Molkov, V., 2019b. Near Field Thermal Dose of Cryogenic Hydrogen Jet Fires. In: Oceedings of the Ninth International Seminar on Fire and Explosion Hazards (ISFEH9). pp. 1360–1366.

Cirrone, D., Makarov, D., Molkov, V., 2019c. Cryogenic hydrogen jets: flammable envelope size and hazard distances for jet fire. In: International Conference on Hydrogen Safety. Adelaide, Australia.

Daubech, J., Hebrard, J., Jallais, S., Vyazmina, E., Jamois, D., Verbecke, F., 2015. Un-ignited and ignited high pressure hydrogen releases : Concentration - Turbulence mapping and overpressure effects. J. Loss Prev. Process Ind. 36, 439–446.

Ekoto, I.W., Ruggles, A.J., Creitz, L.W., Li, J.X., 2014. Updated jet flame radiation modeling with buoyancy corrections. Int. J. Hydrogen Energy 39, 20570–20577.

Friedrich, A., Veser, A., Jordan, T., 2021. PRESLHY D5.4. Summary of experiment series E5.1 (Ignited discharge) results.

Grune, J., 2019. Private communication.

Grune, J., Sempert, K., Kuznetsov, M., Jordan, T., 2013. Experimental study of ignited unsteady hydrogen releases from a high pressure reservoir. Int. J. Hydrogen Energy 39, 6176–6183.

Hankinson, G., Lowesmith, B.J., 2012. A consideration of methods of determining the radiative characteristics of jet fires. Combust. Flame 159, 1165–1177.

Hussein, H.G., Brennan, S., Shentsov, V., Makarov, D., Molkov, V., 2018. Numerical validation of pressure peaking from an ignited hydrogen release....pdf. Int. J. Hydrogen Energy 43, 17954–17968.

Imamura, T., Hamada, S., Mogi, T., Wada, Y., Horiguchi, S., Miyake, A., Ogawa, T., 2008. Experimental investigation on the thermal properties of hydrogen jet flame and hot currents in the downstream region. Int. J. Hydrogen Energy 33, 3426–3435.

Lach, A.W., Gaathaug, A.V., 2021. Large scale experiments and model validation of Pressure Peaking Phenomena-ignited hydrogen releases International Journal of Hydrogen Energy, 46 (11), 2021, 8317-8328.

Lach, A.W., Gaathaug, A.V., Vaagsaether, K., 2020. Pressure peaking phenomena: Unignited hydrogen releases in confined spaces – Large-scale experiments. Int. J. Hydrogen Energy 45,

32702–32712.

Lachance, J., Tchouvelev, A., Engebo, A., 2011. Development of uniform harm criteria for use in quantitative risk analysis of the hydrogen infrastructure. Int. J. Hydrogen Energy 36, 2381–2388.

LaChance, J.L., 2010. Progress in risk assessment methodologies for emerging hydrogen applications. In: Sixth International Short Course and Advanced Research Workshop "Progress in Hydrogen Safety – Regulations, Codes and Standards." Belfast, Northern Ireland, UK.

Magnussen, B., 1981. On the structure of turbulence and a generalized eddy dissipation concept for chemical reaction in turbulent flow. Am. Inst. Aeronaut. Astronaut.

Makarov, D., Shentsov, V., Kuznetsov, M., Molkov, V., 2018. Pressure peaking phenomenon: Model validation against unignited release and jet fire experiments. Int. J. Hydrogen Energy 43, 9454–9469.

Markert, F., Giuliani, L., Sørensen, L.S., Venetsanos, A., Momferatos, G., Rattigan, W., Xu, Z., Grune, J., Gaathaug, A.V., Cirrone, D., Shenstov, V., Kashkarov, S., Makarov, D., Molkov, V., Bouix, D., 2020. HyTunnel-CS Deliverable D3.2 Intermediate report on analytical, numerical and experimental studies on fires.

Miller, D., Eastwood, C.D., Kelly Thomas, J., 2015. Hydrogen jet vapour Cloud explosion: test data and comparison with predictions. In: 11th Global Congress on Process Safety.

Molkov, V., 2012. Fundamentals of Hydrogen Safety Engineering I Download free books at Vladimir Molkov Fundamentals of Hydrogen Safety Engineering I.

Molkov, V., Makarov, V., Bragin, M. V., 2009. Physics and modelling of underexpanded jets and hydrogen dispersion in atmosphere. Phys. Extrem. States Matter 146–149.

Molkov, V. V., Cirrone, D.M.C., Shentsov, V. V., Dery, W., Kim, W., Makarov, D. V., 2021. Dynamics of blast wave and fireball after hydrogen tank rupture in a fire in the open atmosphere. Int. J. Hydrogen Energy 46, 4644–4665.

Murthy, J.Y., Mathur, S.R., 1998. A finite volume method for radiative heat transfer using unstructured meshes. 36th AIAA Aerosp. Sci. Meet. Exhib. M.

Panda, P.P., Hecht, E.S., 2017. Ignition and flame characteristics of cryogenic hydrogen releases. Int. J. Hydrogen Energy 42, 775–785.

Pehr, K., 1996. Aspects of safety and acceptance of LH2 tank systems in passenger cars. Int. J. Hydrogen Energy 21, 387–395.

Peters, N., Rogg, B., 1993. Reduced kinetic mechanisms for applications in combustion systems, Berlin. Berlin.

PRESLHY D6.5, 2021. D6.5 Detailed description of novel engineering tools for LH2 safety, version 2.

Proust, C., Jamois, D., Studer, E., 2011. High pressure hydrogen fires. Int. J. Hydrogen Energy 36, 2367–2373.

Radebaugh, R., 2002. Cryogenics. MacMillan Encycl. Chem.

Reaction Design, I., 2016. Gas-phase Chemical Rate Expressions. CHEMKIN Theory Man. 37–40.

Royle, M., Willoughby, D.B., 2010. Consequences of catastrophic releases of ignited and unignited hydrogen jet releases. Int. J. Hydrogen Energy 36, 2688–2692.

Saffers, J.B., Molkov, V. V., 2013. Towards Hydrogen Safety Engineering for Reacting and non-Reacting Hydrogen Releases. J. Loss Prev. Process Ind. 26, 344–350.

Shih, T.H., Liou, W.W., Yang, A., Shabbir, Z., 1995. A new eddy-viscosity model for high Reynolds number turbulent flows—model development and validation. Comput. Fluids 24, 227–238.

Takeno, K., 2019. Private communication.

Takeno, K., Okabayashi, K., Kouchi, A., Nonaka, T., Hashiguchi, K., Chitose, K., 2007. Dispersion and explosion field tests for 40 MPa pressurized hydrogen 32, 2144–2153.

2.8 LES of cryogenic hydrogen jet flames (UWAR)

In the event of potential liquid hydrogen leaks, the pressurized storage conditions will develop at the leaks, resulting in the formation of under-expanded hydrogen jets. following ignition, a stationary jet fire will develop, resulting in radiative heat flux to the surroundings.

As an example, Warwick FIRE has conducted simulations for the experimental configurations of Hecht and Panda (2019) with hydrogen (inflow) and air (co-flow or zero-flow) injected from the bottom, as shown in Figure 9. The non-reflected boundary conditions were applied on the side boundaries. For the outlet conditions, the parameters were interpolated by assuming first-order derivatives. A stagnant air conditions were imposed at the inlet. The static pressure, P_a, and the static temperature, T_a, of the ambient air were 1 bar and 297 K, respectively.

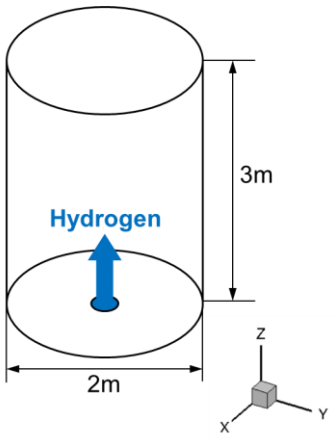

Figure 9. Schematic of computational domain.

UWAR conducted large eddy simulation (LES) of the unsteady ignited cryogenic hydrogen jets using compressible reacting flow solver rhoReactingFOAM within OpenFOAM. Three dimensional (3D) Large Eddy Simulation (LES) with one-equation eddy-viscosity SGS model for compressible flows (Yoshizawa 1993) was used in which a transport equation is solved to resolve the Subgrid Scale (SGS) kinetic energy. The modified version of the eddy dissipation concept (EDC) by Parente(2016) was used to for combustion in conjunction with detailed hydrogen chemistry (9 species and 19 steps) (Ó Conaire 2004). The finite volume discrete ordinates model (FVDOM) was employed to solve the radiative heat transfer equation. The weighted sum of the grey gas model was used to evaluate the gas radiative properties.

Numerical simulations were set up following the boundary and geometric conditions of the PRESLHY experimental measurements:

- the bulk pressure is 200 bar;
- the bulk temperature of released gas is 80 K;
- the nozzle diameter is 4 mm;
- ambient air at 1 bat and 297K;
- stagnant air conditions with a velocity 0 m/s.

Three cases were simulated with different ignition locations as shown in Table 3.

Table 3. Simulation cases

Case	Ignition position, z (m)	Ignition temperature (K)
0.5IG	0.5	2000
1.0IG	1.0	2000
1.0IG	2.0	2000

A comparison of the predicted flame structure for different ignition locations is shown in Figure 10. The characteristic flame temperature approaches the adiabatic combustion temperature T=2260K for stoichiometric hydrogen-air mixture at 80K. Of course, the local flame temperature shown here is not the same as the visible radiant temperature emitted by the flame because the emissivity of the flame is only 3-6% of the total combustion energy. It should be noted that the initial local concentration of hydrogen might be lower than the stoichiometric one, especially near the edges of hydrogen jet. For instance, adiabatic combustion temperature for 15% hydrogen in air at 80K is 1280K. The factor leading to the increase of adiabatic combustion temperature is the local initial temperature of hydrogen – air mixture due to the entrainment of warm air and cold hydrogen. For instance, the equilibrium temperature of 15% hydrogen-air mixture of about 270K leads to higher adiabatic combustion temperature 1450K.

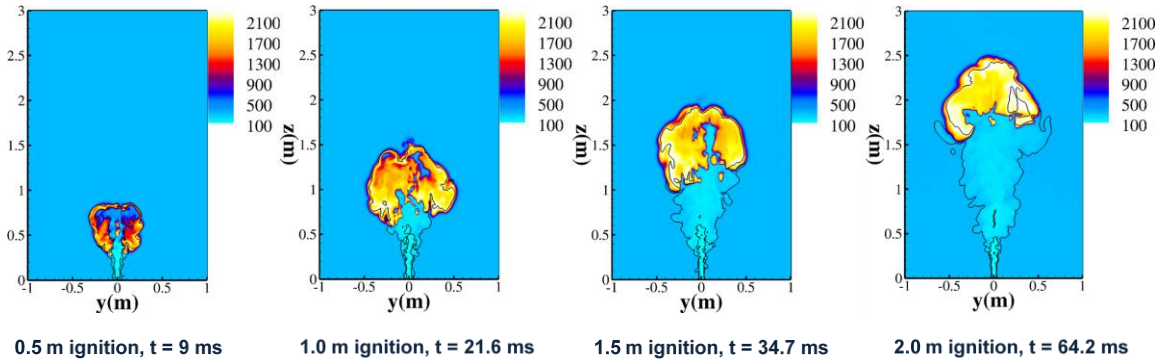

Figure 10. Temperature contours (K) at the *y*-*z* plane. Black iso-lines denote concentrations within the flammability limit, Mol_{H2} = 0.040 - 0.756.

A temporal distribution of OH radical indicates the dynamics of reaction zone in the case of 0.5 m ignition position as shown in Figure 11. It can be seen from the predicted flame structure for different ignition locations in Figure 10 that the predicted characteristic flame temperature approaches the adiabatic combustion temperature T=2260K for hydrogen-air mixtures at 80K. Of course, the local flame temperature shown here is not the same as the visible radiant temperature emitted by the flame because the emissivity of the flame is only 3-6% of the total combustion energy. The predictions for the ignition position of 2m which was further away from the jet exit shows more stable continuous reaction zone as shown in Figure 12. This is thought to be due to the higher level of mixing between the ejected hydrogen and the surrounding air.

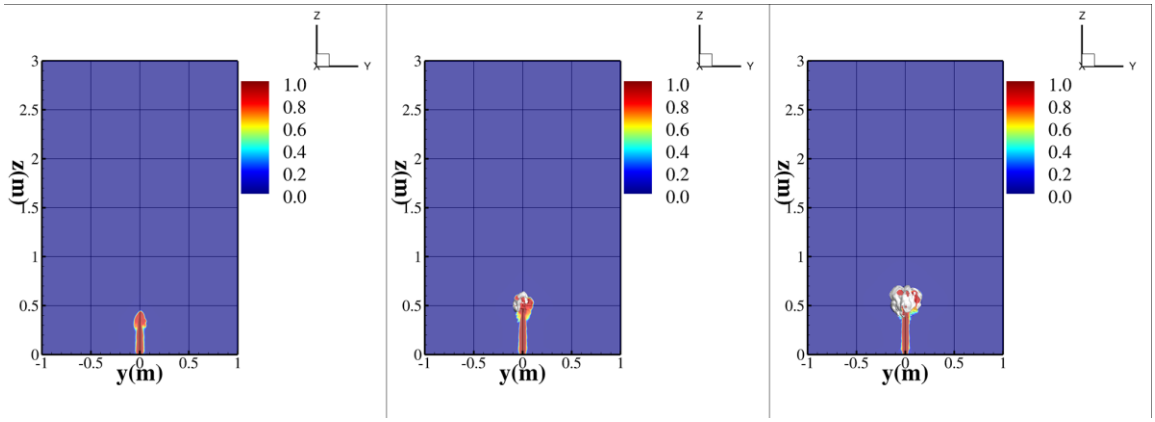

Figure 11. Distributions of H_2 mole fraction, from left to right: time = 2 ms, 3 ms, 4 ms. Iso-surface (white color) of OH mass fraction (0.003) to indicate the reaction zone in case of 0.5 m ignition position.

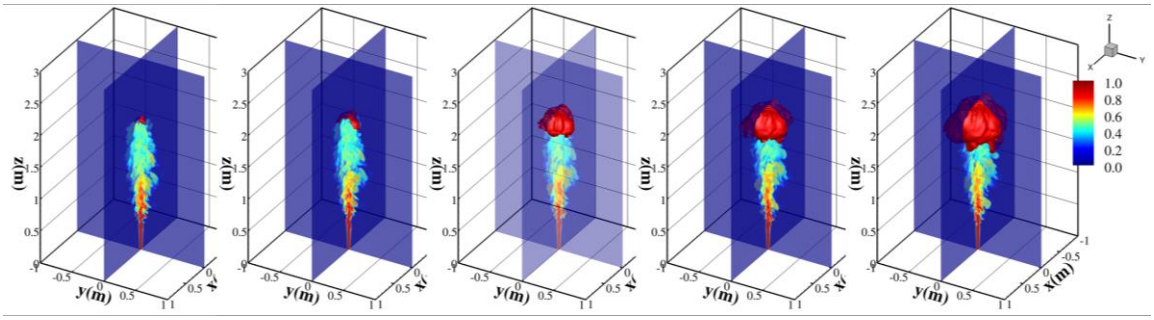

Figure 12. Distributions of H_2 mole fraction, from left to right: time = 0.037s, 0.039s, 0.041s, 0.043s, 0.045s. Iso-surface (red color) of OH mass fraction (0.005) to indicate the flame front in case of 2 m ignition position.

The instantaneous distributions of the temperature are shown in Figure 13. The ignition hot spot is located 1.0 m from the nozzle. Spotted flame kernels are initially formed around the jet tip, and then propagate only outwards rather than downwards towards the main jet body. This is thought to be due to the relatively low temperature of the hydrogen, which impedes the chemical reaction on the jet tip. As a result, the flame propagates to the sides of the jet with expanding flame area as shown by the snapshots from 12 ms to 17 ms. It is also interesting to note that from about 15 ms onwards, the flame kernel also started to propagate inwards towards the main body of the jets due to a combination of further mixing between the hydrogen and air underneath the jet tip and the increase in its temperature with the development of the flame kernels in the outer area of the jets.

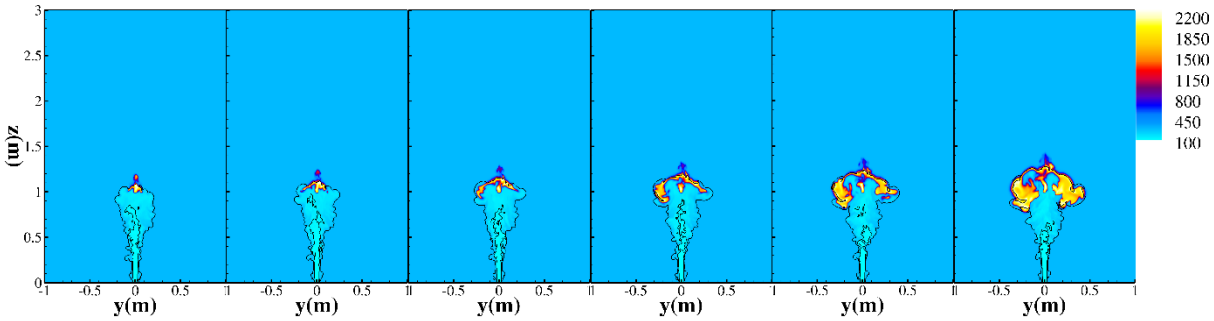

Figure 13. Development of the flame kernel for ignition at 1.0 m with the time step 1 ms from 12 ms to 17 ms. Here the contours are plotted from the predicted temperature (K) and the black iso-lines denote regions with the flammability limit, $MolH_2$ = (0.040, 0.756).

For ignition at 1.5 m, Figure 14 shows the formation and evolution of the flame kernel. The hydrogen jet interacts with the hot spot and induces a flame kernel, as shown by the snapshot at t = 25 ms. Comparing with the predictions for ignition at 1.0 m, the flame kernel not only propagates towards the jet centre but also spreads outwards to envelop the jet tip. The predicted temperatures of the jet tip are also higher due to increasing mixing of hydrogen and air, which led to increased reactivity and flame spread to the core region of the jet. An envelope flame is formed to wrap the jet tip, as depicted by the flame structure at time t = 31 ms.

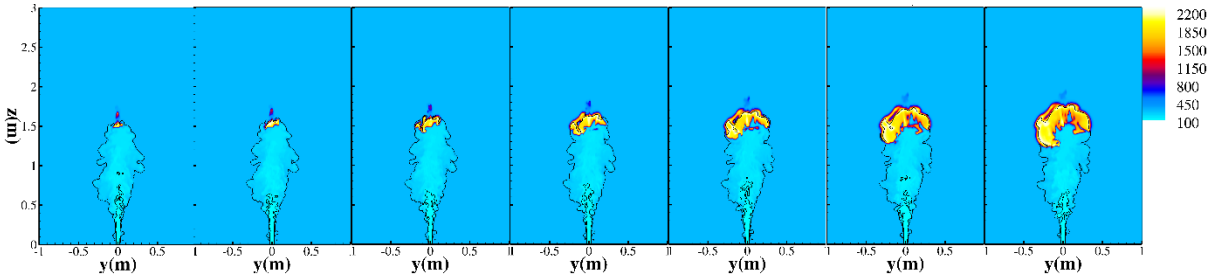

Figure 14. Development of flame kernel for ignition at 1.5 m from 25 ms to 31 ms. Here the contours are plotted from the predicted temperature (K) and the black iso-lines denote regions within the flammability limit, Mol_{H2} = (0.040, 0.756).

In summary, the numerical predictions conducted by UWAR show that for ignition close to the jet exit at 1.0m, the flame cannot propagate inside the cold jet and a side flame is formed; while for ignition at 1.5m, an envelope flame around the jet is formed, which is attributed to increasing mixing between hydrogen and air as well as comparatively higher jet temperature in the downstream region. The unsteady flame dynamics are determined by the complex interactions among turbulence, fuel-air mixing at cryogenic temperature, and chemical reactions.

2.8.1 References

Hecht E. S. and Panda P. P., Mixing and warming of cryogenic hydrogen releases, Int. J. Hydrogen Energy, vol. 44, pp. 8960–8970, 2019.

Ó Conaire M, Curran H J, Simmie J M, et al. A comprehensive modeling study of hydrogen oxidation. International journal of chemical kinetics, 2004, 36(11): 603-622.

Parente A, Malik M R, Contino F, et al. Extension of the Eddy Dissipation Concept for turbulence/chemistry interactions to MILD combustion. Fuel, 2016, 163: 98-111.

Ren Z., Wen J.X., Numerical characterization of under-expanded cryogenic hydrogen gas jets. AIP Advances, 2020, 10(9): 095303.

Yoshizawa A. Bridging between eddy-viscosity-type and second-order turbulence models through a two-scale turbulence theory. Physical Review E, 1993, 48(1): 273.

2.9 Modelling on flame propagations in turbulent hydrogen jet from a high pressure vessel (KIT)

2.9.1 Introduction

Existing studies mainly focused on the hydrogen jet flames after the fire stabilized. The flame propagation and development processes have not been well studied. A complex interaction between turbulence, chemical reaction, and ignition parameters determines the flame development and propagation after ignition. Veser [9] and Friedrich et al. [10] carried out ignition experiments for room temperature and cryogenic hydrogen jets. The flame propagations were observed using a Background Oriented Schlieren (BOS) system. Depending on the ignition location three different flame modes were identified: ignition flash-back to the nozzle followed by a stable jet flame, stable lifted flame without flash-back, and unstable transient flame with quenching. The thresholds hydrogen concentrations between the three flame propagation regimes were 11% and 5% correspond to the distance from the nozzle. In the experiment, the hydrogen mass flow rate remained stable during the leakage. However, when hydrogen releases from a pressurized vessel with a given volume, the stagnation state and mass

flow rate change with time. Therefore, the stagnation state time histories and the flame propagations need to be further studied for the release and ignition of hydrogen stored in a pressurized vessel.

In this paper, the hydrogen releases and ignition were studied for hydrogen released from a pressurized vessel through a circular nozzle and then ignited at 40 cm away from the nozzle. The nozzle had a 4 mm inner diameter. The hydrogen storage vessel volume was 2.815 L with an initial pressure of 5 bar and temperature of 293 K. The hydrogen was ignited at 80 ms after the leakage. The pressure decreases in the vessel were measured. The leakage and flame propagation processes were visualized by a BOS system. Then, the hydrogen leakage and combustion processes were modeled using the parallel CFD code GASFLOW-MPI. The combustion model constants were adjusted and the hydrogen flame propagations were reproduced.

2.9.2 Experimental facility

The experimental investigation of hydrogen releases and combustion was carried out with the DisCha- facility at Karlsruhe Institute of Technology (KIT). The DisCha facility mainly consisted of a stainless steel pressure vessel with an internal free volume of 2.815 L and a weight of about 28 kg, as shown in Figure 15. The vessel was equipped with several ports for instrumentation on its top and a rod that points on a force sensor on its rear side. Opposite to the force sensor, a tubular exhaust pipe was welded to the vessel, where release nozzles with different aperture sizes can be fastened. A nozzle with an inner diameter of 4 mm was used in this experiment. The nozzle was 1 m above the ground.

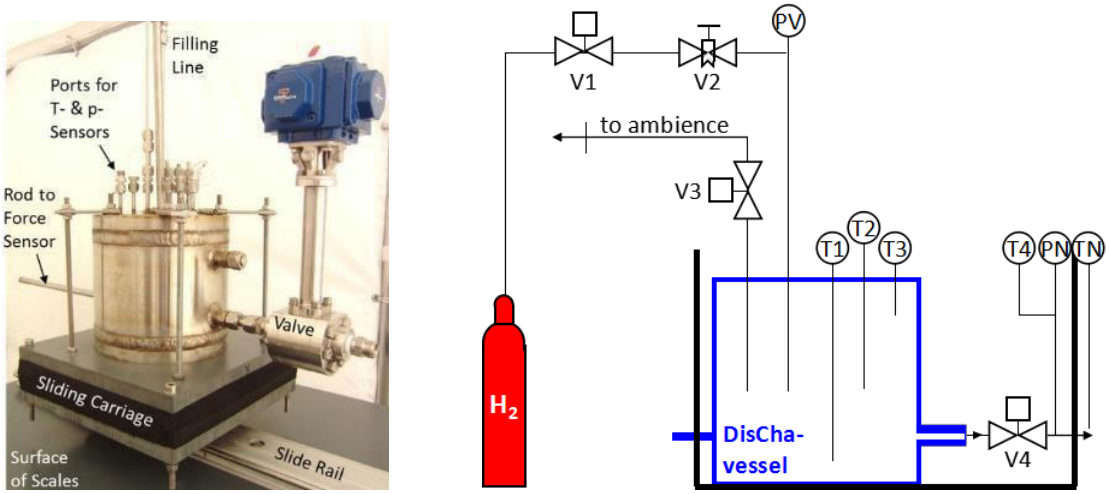

Figure 15. Experimental facility, gas system.

One static pressure sensor (PV in Fig. 1) in the filling line was used to control the initial pressure inside the vessel during the filling procedure and to capture the pressure decrease inside the vessel during the experiment. A second pressure sensor (PN in Figure 15) measured the pressure changes in the release line. Since the second sensor was connected to the tube in between the release valve and the nozzle, the first increase in this signal corresponds to the actual start of the release. NiCr/Ni-thermocouples (Type K, diameter 0.36 mm) were installed inside the vessel to record the gas temperature during the experiment at different heights. The Background Oriented Schlieren (BOS) technique was used to monitor the hydrogen jets and flame propagations. The BOS technique was based on the optical deformation of a background pattern due to density gradients in the gas system under investigation, which was described in [11]. The method was similar to the Schlieren technique and effective for gases with a prominent density difference like hydrogen jet into the air and for combustion processes. A CCD camera was used to record the images followed by digital image processing.

The initial vessel pressure was 5 bar with a temperature of 293 K. The hydrogen was released from the nozzle and then ignited at 80 ms after the leakage. The ignition point was 40 cm away from the nozzle.

2.9.3 Numerical Models

GASFLOW-MPI is a parallel CFD code developed at KIT and has been validated for predicting transport, mixing, and combustion of hydrogen and other gases [12-14]. Implicit Continuous Eulerian- Arbitrary Lagrangian-Eulerian solution algorithm (ICE'd ALE) is used in GASFLOW-MPI to solve the three dimensional compressible Navier-Stokes equations. The Arbitrary-Lagrangian-Eulerian (ALE) technique applies to flows from supersonic to the incompressible limit [15]

2.9.3.1 Turbulence Model

The *k-ε* turbulence model was used. The turbulence kinetic energy, *k*, and its rate of dissipation, *ε*, are obtained from the following transport equations

$$\frac{\partial(\rho k)}{\partial t}+\nabla\cdot(\rho k\boldsymbol{u})=\nabla\cdot\left[\left(\mu_l+\frac{\mu_t}{\sigma_k}\right)\nabla k\right]+P_k+P_{kb}-\rho\varepsilon \quad (1)$$

$$\frac{\partial(\rho\varepsilon)}{\partial t}+\nabla\cdot(\rho\varepsilon\boldsymbol{u})=\nabla\cdot\left[\left(\mu_l+\frac{\mu_t}{\sigma_\varepsilon}\right)\nabla\varepsilon\right]+C_{\varepsilon1}\frac{\varepsilon}{k}(P_k+P_{kb})-C_{\varepsilon2\rho}\frac{\varepsilon^2}{k} \quad (2)$$

where ρ is the density, $\boldsymbol{u}$ is the velocity, t is time, μ_l is the molecular viscosity and the turbulent viscosity, μ_t, can be written as [16]

$$\mu_t=C_\mu\rho k^2/\varepsilon \quad (3)$$

P_k is the turbulence generation due to the viscous forces calculated as

$$P_k=-\frac{2}{3}\rho k\nabla\cdot\boldsymbol{u}-\frac{2}{3}\mu_t(\nabla\cdot\boldsymbol{u})^2+\mu_t\nabla\boldsymbol{u}\cdot(\nabla\boldsymbol{u}+(\nabla\boldsymbol{u})^T) \quad (4)$$

P_{kb} is the turbulence production term due to the buoyancy calculated as

$$P_{kb}=-\frac{\mu_t}{\sigma_b}g\cdot\nabla\rho$$

The constants in the *k-ε* model

$$C_{\varepsilon1}=1.44,\ C_{\varepsilon2}=1.92,\ C_\mu=0.09,\ \sigma_k=1.0,\ \sigma_\varepsilon=1.3.$$

2.9.3.2 Combustion Model

A simple one-step global chemical kinetics model was used, which simplifies the actual chemical processes [17]. In the present implementation of this model, the only reaction modeled is

$$2H_2+O_2\rightarrow H_2O.$$

The transport equation of the density-weighted mean reaction progress variable is solved to model the flame front propagation.

$$\frac{\partial(\rho\xi)}{\partial t}+\nabla\cdot(\rho\xi\boldsymbol{u})=\nabla\cdot\left[\left(\mu_l+\frac{\mu_t}{Sc_t}\right)\nabla\xi\right]+\rho S_\xi \quad (6)$$

where *Sct* is the turbulent Schmidt number, ξ is the reaction progress variable, which is 1 in the burnt mixture and 0 in the unburnt mixture. The key to this modeling approach is the source term,

ρS_ξ Eddy dissipation model (EDM) is based on the assumption that combustion occurs at small scales, where mixing occurs on a molecular level and the rate is assumed to be proportional to the inverse of the turbulent time scale [18]. It was developed from the original eddy break-up model, where the most significant difference is that the EDM model accounts for the fact that the reaction rate cannot occur unless both fuel and oxidizer mix on a molecular scale at a sufficiently high temperature. This is accomplished by relating the reaction rate to the limiting species. In GASFLOW MPI, the model is written as

$$\rho S_\xi = B_1 \rho \frac{\varepsilon}{k} \min\left(Y_{H_2}, \frac{Y_{O_2}}{\varphi}, B_2 \frac{Y_{H_2O}}{1+\varphi}\right) \quad (7)$$

where Y is the local mass fraction of each species and φ is the equivalence ratio. $B1$ and $B2$ are constants that may depend on the structure of the flame and the rate of reaction between hydrogen and oxygen. The model constants $B1$ and $B2$ need to be adjusted on a case-by-case basis [19]. The EDM combustion model has been tested on both turbulent premixed and jet diffusion flames with good results with constants $B1$=4 and $B2$=0.5 [18]. However, for turbulent premixed diffusion flames, constants $B1$ and $B2$ were adjusted to be multiplied by 8 [18]. In this study, the flame propagates in the free turbulent hydrogen jet in presence of non-uniform flow velocity and hydrogen distribution. The model constants may need to be adjusted for such a complex and unique combustion process. The EDM combustion model was used with constant $B1$ of 4, 40, 50, and 100 in this study, and the effects of constant $B1$ were analyzed.

2.9.3.3 Geometry and Grid

The computational domain is shown in Figure 16(a). The hydrogen was released from a pressurized vessel through a circular nozzle and then ignited 40 cm away from the nozzle. The hydrogen storage vessel volume was 2.815 L with an initial pressure of 5 bar and temperature of 293 K. The nozzle's inner diameter was 4 mm, which was enlarged to 7.5 mm for the calculation, mainly considering the computational cost. A sub-grid mass flow rate model was used at the nozzle outlet to ensure the identity of the actual mass flow. A frictionless adiabatic solution for the mass flow rate of hydrogen release is provided as

$$m = \begin{cases} C_d \cdot A \sqrt{\gamma p_1 \rho_1 \left(\frac{2}{\gamma+1}\right)^{\frac{\gamma+1}{\gamma-1}}} & ; \frac{p_2}{p_1} < \left(\frac{2}{\gamma+1}\right)^{\frac{\gamma}{\gamma-1}} \\ C_d \cdot A \sqrt{2 p_1 \rho_1 \left(\frac{\gamma}{\gamma-1}\right)\left[\left(\frac{p_2}{p_1}\right)^{\frac{2}{\gamma}} - \left(\frac{p_2}{p_1}\right)^{\frac{\gamma+1}{\gamma}}\right]} & ; \frac{p_2}{p_1} \geqslant \left(\frac{2}{\gamma+1}\right)^{\frac{\gamma}{\gamma-1}} \end{cases} \quad (8)$$

where A is the computational nozzle area. Cd is the discharge coefficient, which is the ratio of the actual area and computational area and equals 0.284 in this study. $p1$ and $\rho 1$ are the pressure and hydrogen density in the vessel, $p2$ is the ambient pressure, and the specific heat ratio of hydrogen γ=1.4.

The computational domain was discretized using hexahedral elements, with 211x118x211 grids at x, y, and z direction. Very fine grids were used around the nozzle exit to ensure convergence and calculation accuracy as shown in the cross-sectional view of the mesh in Figure 16(b). The ambient air temperature was 293 K and the ambient pressure was 1.0 bar.

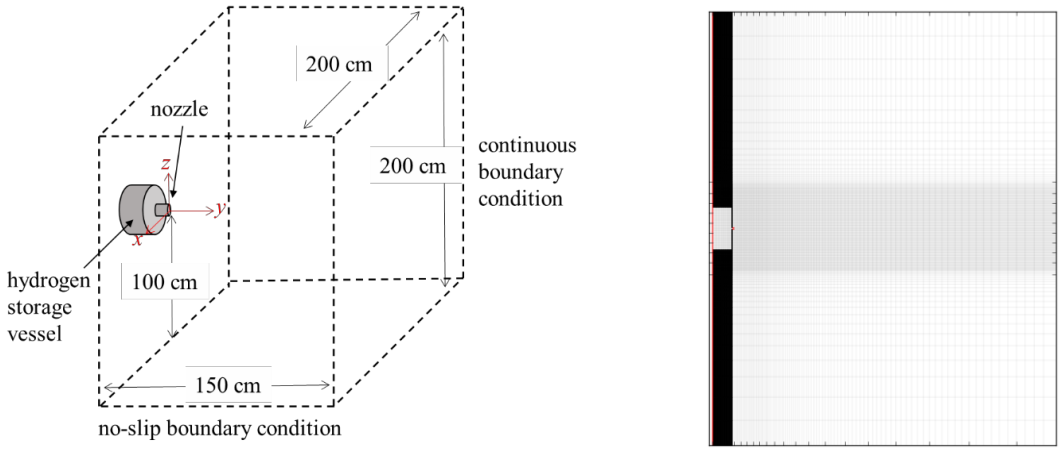

(a) Computational domain (b) Cross-sectional view of the mesh

Figure 16. Computational domain and mesh.

2.9.4 Results and discussion

2.9.4.1 Hydrogen Release and Distribution before Ignition

The storage vessel pressure dropped from 5 bar to 3.46 bar during the release as shown in Figure 17, which was well predicted by GASFLOW-MPI. The calculated vessel pressure was 3.30 bar at 80 ms, with an error of 4.62%. The measured and calculated hydrogen jets at 80 ms after the leakage are shown in Figure 18. The hydrogen diffusion regions agree well although the exact concentration values have not been measured by the BOS system. The calculated jet centerline hydrogen mole fractions and velocities at 80 ms are shown in Figure 19. The distribution of hydrogen mole fraction fluctuated due to the instantaneous turbulent.

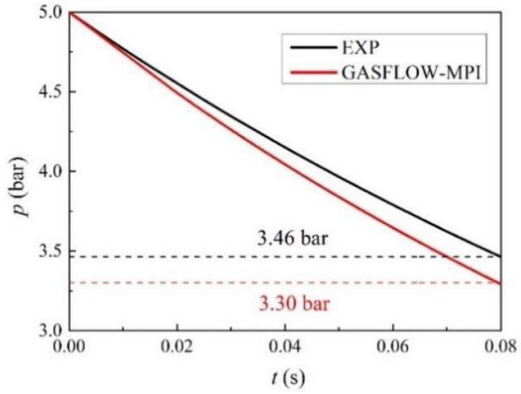

Figure 17. Storage vessel bulk pressure.

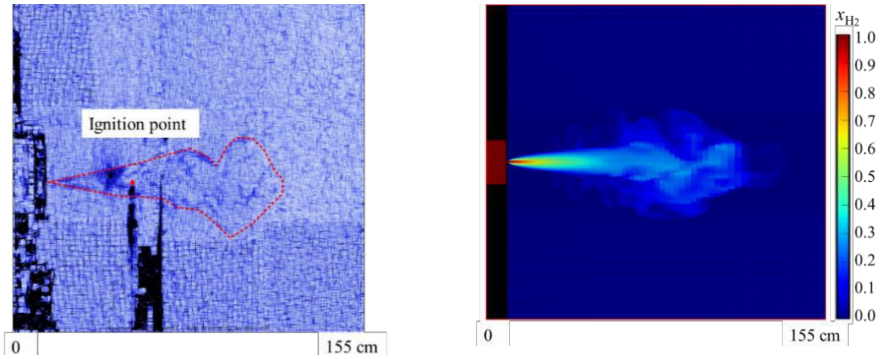

(a) Experimental (b) The calculated hydrogen volume fraction

Figure 18. Hydrogen jet at 80 ms after leakage.

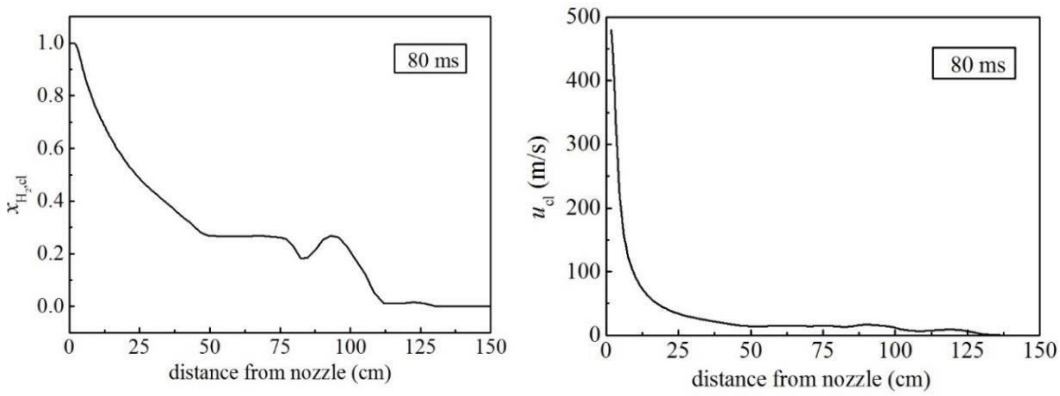

(a) Centerline hydrogen mole fractions (c) Centerline velocities

Figure 19. Centerline hydrogen mole fractions and velocities at 80 ms.

2.9.4.2 Hydrogen Flame Propagations

The hydrogen jet was ignited at 40 cm away from the nozzle at 80 ms after the leakage. The complex interaction of turbulence and chemical reaction determined the further progress of the combustion. A sequence of BOS images is shown in Figure 20. After ignition at the indicated ignition point, the flame propagated downstream immediately, while at the same time the turbulent flame front moved towards the nozzle. The flame spread back to the nozzle at 20 ms after ignition. The flame velocity can be calculated as

$$u_{flame} = (L_{i+1} - L_i)/(t_{i+1} - t_i) \quad (9)$$

where Li and Li+1 are the flame edge positions at time ti and ti+1.

The downstream and upstream flame velocities are shown in Figure 21. The downstream flame velocity decayed as the distance from the ignition point increases. The downstream flame velocity was about 65 m/s near the ignition point and decayed to 30 m/s at the distance of 45~60 cm from the ignition point, then decayed below 10 m/s at the distance of 80~100 cm from the ignition point. The upstream flame velocity fluctuated with distance from the ignition point. The average upstream flame velocity within 20 ms after the ignition was 18 m/s.

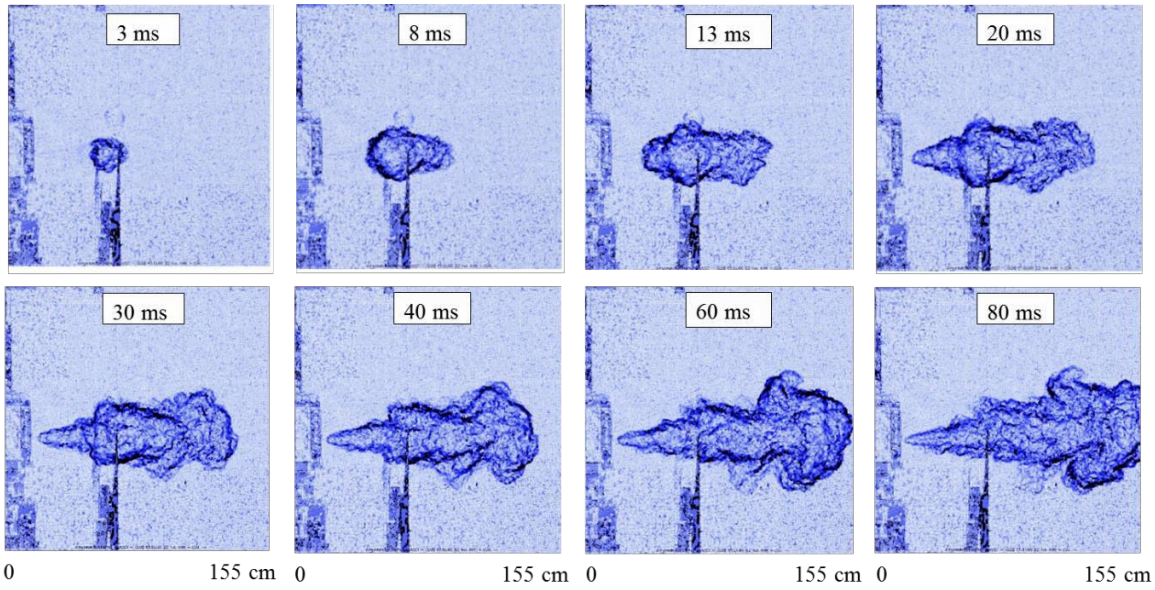

Figure 20. BOS images after ignition.

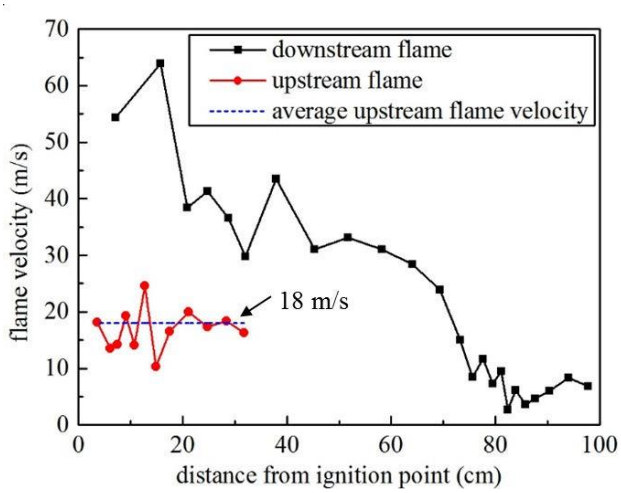

Figure 21. Downstream and upstream flame velocities.

2.9.4.3 Effects of Model Constants

The calculated flame temperature contours at different moments after ignition and the corresponding BOS images are shown in Figure 22~Figure 25. The model constant *B*1 in Eq. (7) significantly affects the calculated flame propagations as shown in. that figures. The flame propagated only downstream without flash-back after ignition for *B*1=4, as shown in Figure 22. For *B*1=40 in Figure 23, the flame propagated downstream and upstream. The flame spread back to the nozzle at 35 ms after ignition with an average upstream flame velocity of 11 m/s, which was lower than the experimental result of 18 m/s. For *B*1=50 in Figure 24, the flame propagated downstream and upstream and spread back to the nozzle at 20 ms after ignition. The predicted average upstream flame velocity was 20 m/s. The flame propagation processes and shapes in Figure 24 show good agreement between the predicted and measured results. For *B*1=100, the flame spread upstream quickly after ignition and takes only 1 ms to propagate to the nozzle, as shown in Figure 25. The upstream flame velocity was as high as 400 m/s, which is much higher than the experimental result.

The calculated flame propagated upstream faster as the model constant *B*1 increases. In this study, the constant *B*1 was adjusted to 50 and the predicted hydrogen flame propagations agreed well with the experimental results. More numerical calculations and experimental verifications need to be further studied for hydrogen jet ignitions to adjust the constants in the EDM model.

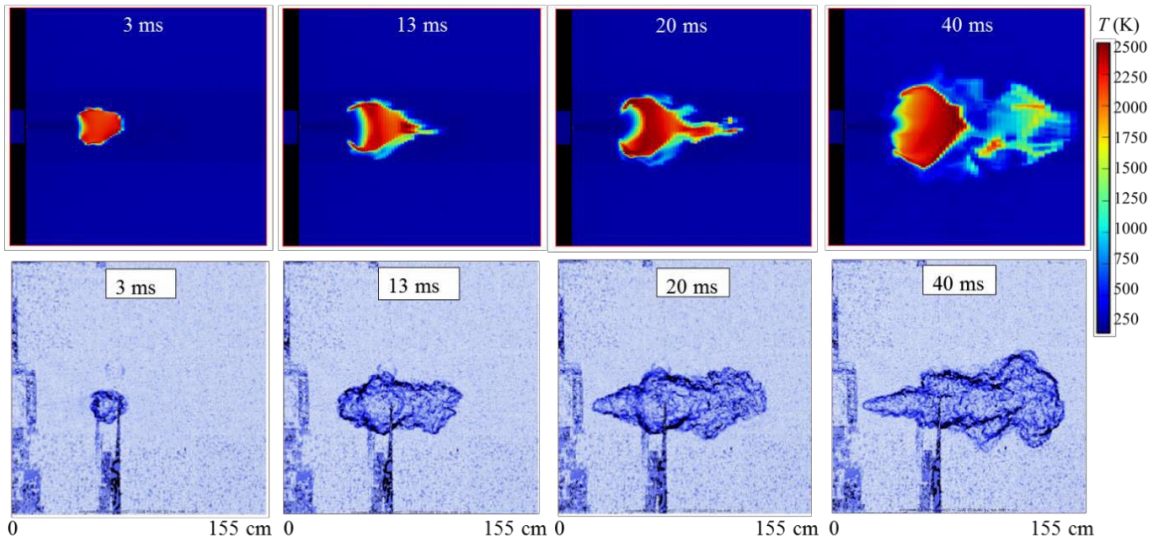

Figure 22. Flame propagations after ignition (up: GASFLOW-MPI (*B*1=4); down: experiment).

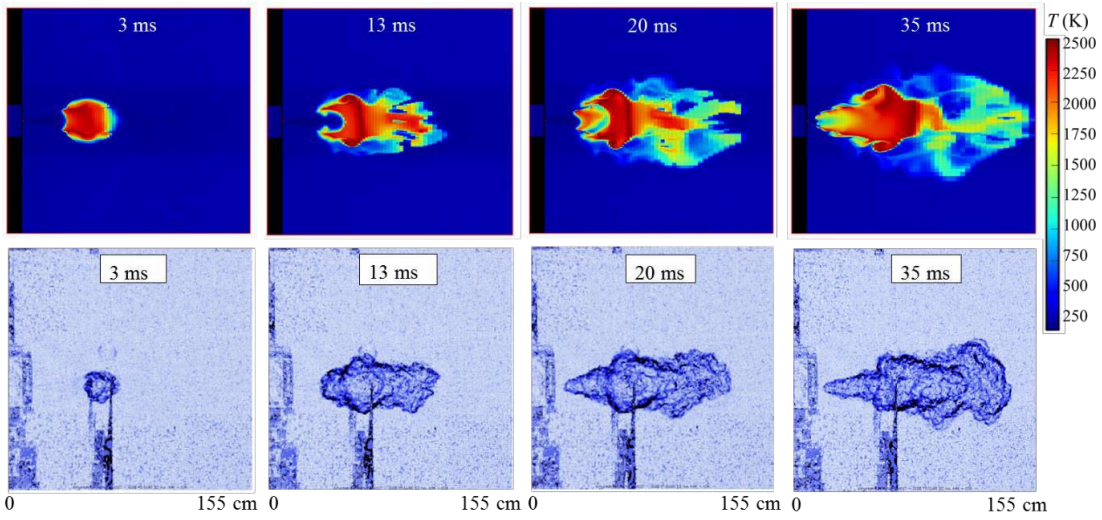

Figure 23. Flame propagations after ignition (up: GASFLOW-MPI (*B*1=40); down: experiment).

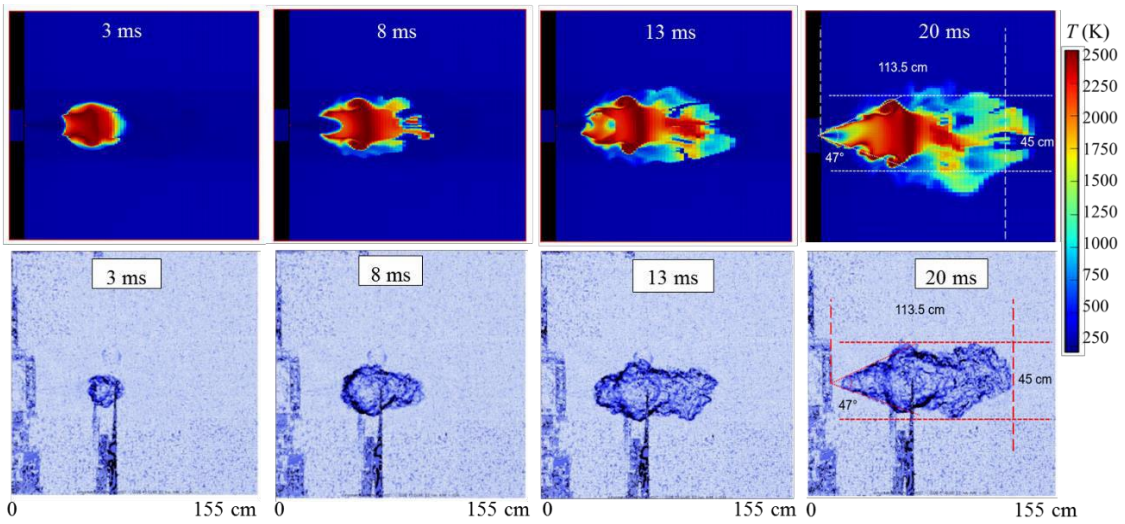

Figure 24. Flame propagations after ignition (up: GASFLOW-MPI (*B*1=50); down: experiment).

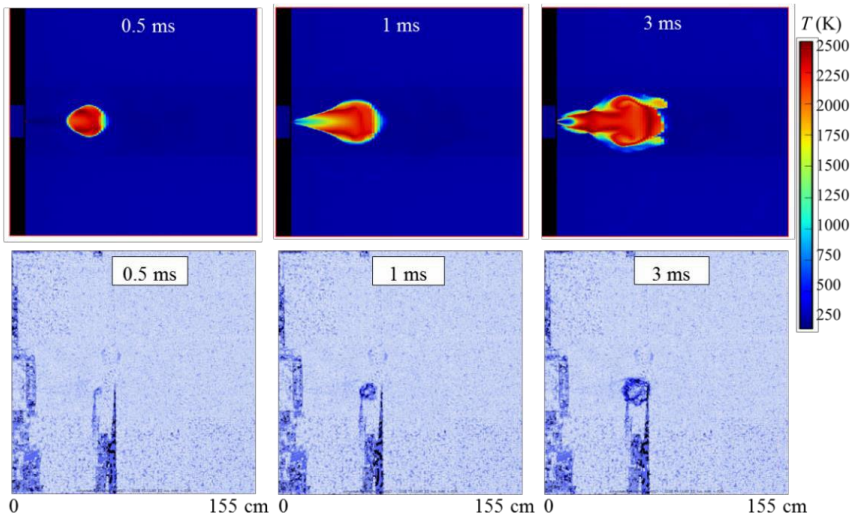

Figure 25. Flame propagations after ignition (up: GASFLOW-MPI (*B*1=100); down: experiment).

2.9.5 Conclusions

This study measured and modeled the hydrogen release and ignition processes. The hydrogen storage vessel volume was 2.815 L with an initial pressure of 5 bar and temperature of 293 K. The hydrogen was ignited at 40 cm away from a nozzle with a 4 mm inner diameter. The CFD models using GASFLOW-MPI solved the three-dimensional, instantaneous Navier-Stokes equations with the k-ε turbulence model and EDM combustion model.

The measured storage vessel pressure dropped from 5 bar to 3.46 bar before ignition, which was well predicted by GASFLOW-MPI. After ignition at the indicated ignition point, the flame propagated downstream immediately, while at the same time the turbulent flame front moved towards the nozzle. The flame spread back to the nozzle at 20 ms after ignition. The downstream flame velocity was measured to be 65 m/s near the ignition point and decayed below 10 m/s at the distance of 80~100 cm from the ignition point, while the average upstream flame velocity was 18 m/s. The calculated flame propagated upstream faster as the constant $B1$ in the EDM combustion model increases. The constant $B1$ was adjusted to 50 in this study. The good agreement between the calculated and experimental data confirms the powerful feature of GASFLOW-MPI in the simulation of hydrogen combustion in the free turbulent jet.

The present results contribute to the evaluation of the accident consequences of hydrogen leakage and combustion.

2.9.6 References

[1] Barbir F., Transition to Renewable Energy Systems with Hydrogen as an Energy Carrier, Energy, 34, No. 3, 2009, pp. 308-312.

[2] Apak S., Atay E. and Tuncer G., Renewable Hydrogen Energy and Energy Efficiency in Turkey in the 21st Century, International Journal of Hydrogen Energy, 42, No. 4, 2017, pp. 2446-2452.

[3] Panwar N. L., Kaushik S. C. and Kothari S., Role of Renewable Energy Sources in Environmental Protection: A Review, Renewable and Sustainable Energy Reviews, 15, No. 3, 2011, pp. 1513-1524.

[4] Schefer R., Houf W. and Bourne B. et al., Spatial and Radiative Properties of an Open-flame Hydrogen Plume, International Journal of Hydrogen Energy, 31, No. 10, 2006, pp. 1332-1340.

[5] Mogi T. and Horiguchi S., Experimental Study on the Hazards of High-pressure Hydrogen Jet Diffusion Flames, Journal of Loss Prevention in the Process Industries, 22, No. 1, 2009, pp. 45-51.

[6] Panda P. P. and Hecht E. S., Ignition and Flame Characteristics of Cryogenic Hydrogen Releases, International Journal of Hydrogen Energy, 42, No. 1, 2017, pp. 775-785.

[7] Brennan S. L., Makarov D. V. and Molkov V., LES of High Pressure Hydrogen Jet Fire, Journal of Loss Prevention in the Process Industries, 22, No. 3, 2009, pp. 353-359.

[8] Makarov D. and Molkov V., Plane Hydrogen Jets, International Journal of Hydrogen Energy, 38, No. 19, 2013, pp. 8068-8083.

[9] Veser A., Kuznetsov M. and Fast G. et al., The Structure and Flame Propagation Regimes in Turbulent Hydrogen Jets, International Journal of Hydrogen Energy, 36, No. 3, 2011, pp. 2351-2359.

[10] Friedrich A., Breitung W. and Stern G. et al., Ignition and Heat Radiation of Cryogenic Hydrogen Jets, International Journal of Hydrogen Energy, 37, No. 22, 2012, pp. 17589-17598.

[11] Klinge F., Kirmse T. and Kompenhans J., Application of Quantitative Background Oriented Schlieren (BOS): Investigation of a Wing Tip Vortex in a Transonic Windtunnel, Pacific Symposium on Flow Visualization & Image Processing. DLR, 2003.

[12] Xiao J., Travis J. R. and Royl P. et al., Three-dimensional All-speed CFD Code for Safety Analysis of Nuclear Reactor Containment: Status of GASFLOW Parallelization, Model Development, Validation and Application, Nuclear Engineering and Design, 301, 2016, pp. 290-310.

[13] Xiao J., Kuznetsov M. and Travis J. R., Experimental and Numerical Investigations of Hydrogen Jet Fire in a Vented Compartment, International Journal of Hydrogen Energy, 43, No. 21, 2018, pp. 10167-10184.

[14] Li Y., Xiao J. and Zhang H. et al., Numerical Analysis of Hydrogen Release, Dispersion and Combustion in a Tunnel with Fuel Cell Vehicles Using All-speed CFD Code GASFLOW-MPI, International Journal of Hydrogen Energy, 46, No. 23, 2021, pp. 12474-12486.

[15] Hirt C. W., Amsden A. A. and Cook J. L., An Arbitrary Lagrangian-Eulerian Computing Method for All Flow Speeds, Journal of Computational Physics, 14, No. 2, 1974, pp. 227-253.

[16] Launder B. E. and Spalding D. B., The Numerical Computation of Turbulent Flows, Computer Methods in Applied Mechanics and Engineering, 3, No. 2, 1974, pp. 269-289.

[17] Mller C., Hughes E. D. and Niederauer G. F. et al., GASFLOW: A Computational Fluid Dynamics Code for Gases, Aerosols, and Combustion, Volume 2: User's Manual, Office of Scientific and Technical Information Technical Reports, 1998.

[18] Magnussen B. F. and Hjertager B. H., On Mathematical Modeling of Turbulent Combustion with Special Emphasis on Soot Formation and Combustion, Symposium on Combustion, 16, No. 1, 1977, pp. 719-729.

[19] Poinsot T and Veynante D. Theoretical and Numerical Combustion. R.T. Edwards, Inc. 2005.